

# New Insight into the Recent Earthquake Activity in North Cambay Basin, Western India: Seismological and Geodetic Perspectives

by Pallabee Choudhury, Sumer Chopra, Charu Kamra, and Archana Das

**Abstract** The intraplate Gujarat region located at the trijunction of three failed rifts, Kachchh, Narmada, and Cambay, is one of the most seismically active intraplate regions of the world. Among these three, the Cambay basin has been investigated thoroughly for petroleum. However, the basin has not been studied from a seismotectonic perspective. For the past few years, the northern part of the Cambay basin is becoming active with reasonably frequent earthquake occurrences. In the past 10 yr, ~995 earthquakes have been recorded from the region with a maximum magnitude up to 4.2. Most of the earthquakes are in the magnitude range 1–3. Since 2009, four Global Positioning System (GPS) stations have been in operation in the vicinity of the Cambay basin, and a maximum deformation of  $1.8 \pm 0.1$  mm/yr has been estimated. The GPS-derived strain rates of  $\sim 0.02\text{--}0.03$  microstrain/yr are prevalent in the region. An average strain rate of 0.02 microstrain/yr in the region can generate an earthquake of magnitude 6.4. The focal mechanisms of the earthquakes have been mostly normal with strike-slip component and corroborated by the geodetic strain tensors. Most of the seismicity is clustered in the basement ridges, striking along pre-existing Precambrian trends that cross the Cambay basin. Complex geodynamics have developed around the northern part of the Cambay rift because of the various movements along several faults, presence of basement ridges, and subsurface plutonic bodies in a failed rift, which are creating stresses and causing earthquakes in this part of the rift. We postulated that the highly heterogeneous subsurface structure beneath the northern part of the Cambay rift is creating additional stress, which is superimposing on the regional stress field substantially, and this mechanism is plausibly facilitating the localized extensional tectonics in the region where compression is expected.

## Introduction

Intraplate earthquakes occur within the interiors of the tectonic plate where strain rates are usually very low. Large earthquakes are less frequent in continental interiors than those along the plate boundaries. The recurrence rate of large earthquakes in the interiors of the tectonic plate is thousands of years (Talwani, 1999). However, it is seen that some of the most damaging earthquakes have occurred within the intraplate regions such as New Madrid ( $M_w$  8.1 in 1811 and  $M_w$  7.8 in 1812), Kachchh ( $M_w$  7.8 in 1819 and  $M_w$  7.6 in 2001), Charleston ( $M_w$  7.3 in 1886), Tangshan ( $M_s$  7.8 in 1976), Haicheng ( $M_s$  7.3 in 1975), and Sudan ( $M_s$  7.2 and 7.0 in 1990) (Gangopadhyay and Talwani, 2003). In India, in addition to Kachchh, where several damaging earthquakes have been recorded in the past, other parts such as Latur ( $M_w$  6.3 in 1993), Bharuch ( $M_w$  5.4 in 1970), Jabalpur ( $M_w$  5.8 in 1997), and Bhadrachalam ( $M_w$  5.7 in 1969) have also witnessed damaging earthquakes during the past century. Gangopadhyay and Talwani (2003), after studying various intraplate earthquakes in different parts of the world,

have postulated that intraplate seismicity mostly occurs in failed rifts along the pre-existing highly stressed zones, named as stress concentrators. These stress concentrators, such as intersecting faults, buried plutons, and rift pillows, are structures where tectonic plate stresses can cause a localized buildup of stresses that are occasionally released in the form of earthquakes (Gangopadhyay and Talwani, 2003).

Gujarat, located in the westernmost part of India and covering an area of around 196,000 km<sup>2</sup>, is seismically one of the most active intraplate regions of the world. It forms a trijunction with three intracratonic rifts, Kachchh, Cambay, and Narmada (Biswas, 1987). According to the Indian code (Bureau of Indian Standards [BIS], 2002), the highest seismic hazard (zone V) is assigned to the region of Kachchh in Gujarat. It is the only region, apart from the Himalaya–Andaman belt, that has high seismic hazard and can generate earthquakes of magnitude  $\geq 8$ . The other parts of Gujarat are seismically less active and are in zones II–IV as per the Indian code (BIS, 2002). The following regions of Gujarat

have witnessed many large and moderate earthquakes along the active faults in the recent past: Indus delta (modified Mercalli intensity [MMI] X in 1668), Kachchh ( $M_w$  7.8 in 1819), Lakhpat (MMI VIII in 1845), Mount Abu (M 5.0 in 1909), Paliyad (M 5.7 in 1938), Anjar ( $M_w$  6.0 in 1956), Palanpur (M 5.0 in 1962), Mount Abu (M 5.5 in 1969), Bharuch ( $M_w$  5.4 in 1970), and Bhuj ( $M_w$  7.6 in 2001), in addition to many small earthquakes (Rajendran and Rajendran, 2001; Rastogi *et al.*, 2013).

The Cambay rift basin (CRB) comes under zones III and IV of the seismic zoning map of India (BIS, 2002). The areas covered by zones III and IV can expect intensities of VII and VIII, respectively, on Medvedev–Sponheuer–Karnik scale. In addition, the expected magnitudes of the maximum credible earthquakes (MCEs) in zones III and IV are 6.0 and 7.0, respectively. A small area in the northwest of the CRB is assigned zone IV, and the rest is assigned zone III. Two noteworthy historical earthquakes occurred in the northern part of Cambay basin in 1848 ( $M_w$  5.7) and in 1969 ( $M_w$  5.5) (Rastogi *et al.*, 2013). The maximum intensity of VII was reported for the 1969 event. The fault plane solution of the 1969 earthquake was a dominant thrust type with subordinate strike-slip component (Chandra, 1978). Another earthquake of magnitude 5.3 occurred just west of the extension of west-coast lineament (Chandra, 1978). Locations of these historical, as well as recent earthquakes as reported by different sources, are shown in Figure 1. Moreover, the Broach earthquake (23 March 1970) with a magnitude of 5.4 occurred near the junction of Narmada, Cambay, Girnar, and Panvel seismic zones. Two alternate fault-plane solutions for this earthquake show thrusting with a component of strike-slip faulting (Chandra, 1977).

The installation of a dense network of broadband stations in the Gujarat region (Chopra *et al.*, 2008; Rastogi *et al.*, 2013) after the 2001 Bhuj earthquake has enabled the monitoring of seismicity at microlevel in Gujarat and in adjoining regions. The network installed by the Institute of Seismological Research (ISR) has been in operation since 2006. The analysis of the past 10 yr data indicates that the northern part of the Cambay basin has increased seismic activity, with many small earthquakes recorded from this part of the basin. In 2010 and 2017, two earthquakes of  $M_w$  4.2 and 4.1, respectively, occurred in this region. In addition, ~29 earthquakes of magnitude between 3 and 4 have been recorded from this region since 2007. Historically, the region has witnessed many earthquakes of magnitude 4–5 (Rastogi *et al.*, 2013).

The CRB has been thoroughly investigated with regard to petroleum and to understand the shallow subsurface geology. However, frequent seismic activity in the northern part of Cambay basin makes it important to investigate the cause of earthquakes, which has not been addressed so far. In this work, we collected seismicity information and estimated focal mechanism of several minor to light earthquakes. Four Global Positioning System (GPS) stations deployed by the ISR have also been running in the vicinity of the CRB since

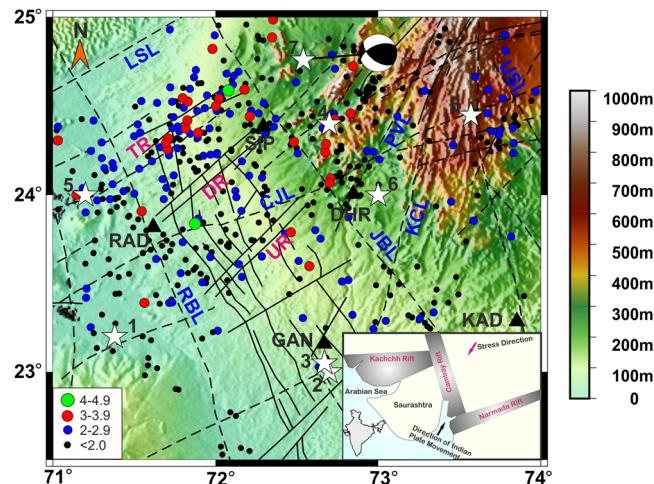


**Figure 1.** Seismotectonic map of the Cambay basin and adjoining areas. Triangles represent the locations of BBS stations installed by Institute of Seismological Research (ISR). Black, blue, red, and green circles indicate locations of M 1.0–1.9, 2.0–2.9, 3.0–3.9, and 4.0–4.9 earthquakes, respectively, as shown in the key. Open stars depict epicenters of historical as well as earthquakes recorded in the recent past before the inception of ISR seismic network. 1, 1882 M 3.5; 2, 1897 M 3.7; 3, 1898 M 4.3; 4, 1906 M 4.3; 5, 1950 M 5.3; 6, 1962 M 4.6; 7, 1969 M 5.5; 8, 1986 M 4.1. (Inset) Regional tectonic map of Gujarat (after Biswas, 2005). The lineaments are shown by dashed lines. CJL, Chambal–Jamnagar; DR, Diyodar ridge; JBL, Jaisalmer–Barwani; KCL, Kishangarh–Chipri; LSL, Luni–Sukri; PVL, Pisangan–Vaditagan; RBL, Radhanpur–Barmer; TR, Tharad ridge; UR, Unhawa ridge; USL, Udaipur–Sardarpur. The color version of this figure is available only in the electronic edition.

2009. We calculated the strain rates from the GPS observations and the magnitude of the maximum potential earthquake in this region. We correlated the seismological and geodetic observations to find out the cause of earthquakes in this region, with the support of the results of previous studies.

## Evolution and Tectonics of the CRB

The continued ridge push because of the spreading of the Arabian seafloor, the collision of the Indian plate with the Eurasian plate, and slab pull from the Andaman–Sumatra trench cause the anticlockwise rotation of the Indian tectonic plate, creating maximum horizontal compression in north-northeast–south-southwest direction and reactivation of rifts (Biswas, 2014). Two sets of faults trending north-northwest–south-southeast and east-northeast–west-southwest are dominant in the northern part of the western continental margin of India (WCMI) comprising Cambay, Kachchh, and Narmada rifts. The former is formed because of intercontinental rifting, and the latter is caused by intraplate pericratonic rifting. The northern part of the WCMI, comprising these three pericratonic rifts, is highly strained because of its proximity to Mekran thrust and transverse faults such as Owen fracture zone, Murray ridge, Ornach–Nai, and Chaman fault zones (Biswas, 2014). The Nagar Parkar fault (NPF), which is

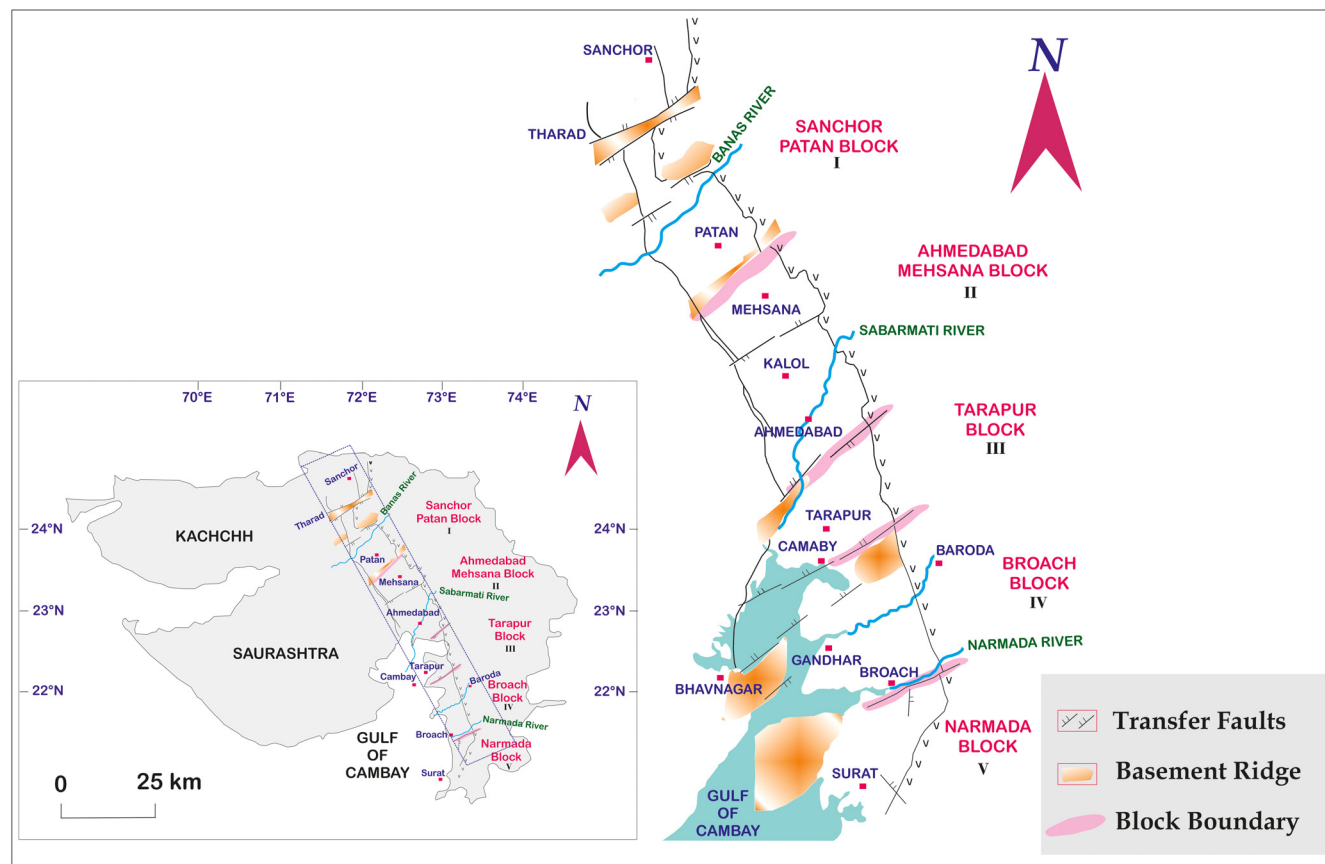


**Figure 2.** Tectonic map of Cambay rift (modified after Wani and Kundu, 1995; Biswas, 2012). Inset shows the location of the Cambay rift (marked by dotted rectangle) with reference to the Gujarat region. The color version of this figure is available only in the electronic edition.

the northern shoulder of the Kachchh rift, segments the southern part of the Indus shelf. The NPF appears to be a transform fault, and its motion is induced by the rotation of the Indian plate. The rotation activates the existing faults, and the north-northeast–south-southwest compression inverts the rift faults into transpressional strike-slip faults. All these three rifts with deep-seated plutons undergo structural inversion and are potential areas for strain accumulations (Biswas, 2014). The western continental margin of the Indian plate has evolved because of the rifting along the major Precambrian trends, such as north-northwest–south-southeast Dharwar, northeast–southwest Aravalli–Delhi, and east-northeast–west-southwest Satpura, giving rise to these three rift basins. The present-day structure of the CRB is influenced by these three trends (Biswas, 1982; Kundu and Wani, 1992). The Cambay rift comprises three principal structures: the extensional faults developed during rifting, asymmetric half-grabens, and transfer zones (Kundu and Wani, 1992). Two types of extensional faults are formed during rifting: north–south to north-northwest–south-southeast-trending listric normal faults and northeast–southwest to east-northeast–west-southwest-trending transfer faults following Dharwar and Aravalli–Delhi trends (Kundu and Wani, 1992). The CRB is bounded by steep north-northwest–south-southwest-trending, discontinuous faults, east

Cambay basin margin, and west Cambay basin margin (WCBM) that restrict the width of the basin. From north to south, the CRB is dissected into several blocks by transverse faults, oriented in an east–west or east-northeast–west-southwest direction (Fig. 2). Some of these faults are old and deep-rooted and extended down to the Precambrian basement (Gupta, 1981).

The basin is divided into five tectonic blocks (the Narmada, Jambusar–Broach, Cambay–Tarapur, Ahmedabad–Mehsana, and Patan–Tharad–Sanctor blocks) (Mathur *et al.*, 1968), as shown in Figure 2. All five blocks have a different level of tectonic activity, controlled by the basement faults. These blocks are separated by transfer zones consisting of discontinuous ridges (Kundu and Wani, 1992). The Cambay basin narrows toward the north but tectonically continues beyond Sanctor to pass into the Barmer basin of Rajasthan. The Aravalli and Delhi trends, which cross the Cambay graben, are seen as important cross trends within the graben in the form of numerous transverse and oblique faults, uplifts, and geomorphic lineaments (Biswas, 1987). The Patan–Tharad–Sanctor block is bounded by Banas river in the south, and its northern boundary is a few kilometers north of Sanctor town area. This block is characterized by the presence of three major depressions separated from each other by narrow transverse ridges. Near Tharad, a dominant east-northeast–west-southwest

to east–west lineament trend has been reported, implying the continuation of the Aravallis in the subsurface. These lineaments signify the fault-bounded intrabasinal horst and grabens within the Cambay basin. The faults in the sediments and at the Deccan Trap level are all steep dipping. In most of the cases, the faults are linear.

### Estimation of Magnitude, Frequency of Occurrence, and Focal Mechanism of Earthquakes

After the 2001 Bhuj earthquake, a dense network of broadband seismographs (Gujarat seismological network [GSNet]) was established in Gujarat (Chopra *et al.*, 2008). The network was started with 23 stations in 2006, which was strengthened to 48 in 2008 and to 54 in 2014. Most of the stations were in Kachchh (west of Cambay basin) because the region is seismically most active. Of the 54 stations, the following five are located in Cambay basin: Radhanpur (RAD), Gandhinagar (GAN), Kadana (KAD), Sipu (SIP), and Dharoi (DHR). These stations are permanent and have been in operation since 2006. The data are received in real time through a very small aperture terminal and then analyzed using the SEISAN software (Havskov and Ottemöller, 1999). The earthquake parameters such as epicenter and magnitude were estimated using SEISAN (Havskov and Ottemöller, 1999). The catalog of earthquakes, which includes historical seismicity documented by various agencies or authors, shows that a total of 1006 earthquakes (of magnitude 1.0–5.7) were recorded from 1840 to 2017 in the northern part of the Cambay basin and the adjoining regions (Fig. 1). Since the inception of the ISR network, a total of 995 earthquakes (of magnitude 1.0–4.2) were recorded in this region. Of these, 398 earthquakes had their epicenters inside the Cambay rift (Fig. 1).

A quantitative approach to seismicity analysis can be conducted with the assessment of seismicity parameter (*b*-value) obtained from the frequency–magnitude distribution given by the Gutenberg–Richter relation (Gutenberg and Richter, 1944):

$$\log_{10}N = a - bM, \quad (1)$$

which *N* is the cumulative frequency of the occurrence of the magnitude **M** in a given earthquake database. The intercept and slope (*a*- and *b*-value) signify the background seismicity level and the magnitude of size distribution, respectively. A high *b*-value of  $1.08 \pm 0.04$  is estimated for the region (Fig. 3a), implying that the majority of the earthquakes are of lower magnitude. Assigning the magnitude of completeness (*M*<sub>c</sub>) to instrumental earthquake catalog is essential for seismicity analysis. The *M*<sub>c</sub> of earthquakes in the region is estimated using the maximum curvature technique (Weimer and Wyss, 2000) as shown in Figure 3a. We found that the catalog is complete for a magnitude of  $\geq 1.6$  since 2006 in the region. In addition to two earthquakes of magnitude  $> 4$  (*M*<sub>w</sub> 4.2 and 4.1), the region has recorded 180 events of

magnitude 2–3 and 29 events of magnitude 3–4 since 2007. The activity was high in 2007, 2010, 2014, 2016, and 2017 (Fig. 3b). If we separate the earthquakes regionwise, it is noted that the Tharad ridge and its adjoining region are the most active part of the Cambay rift at present because many events are clustered in and around the ridge. Since 2006, the region around Tharad has recorded 214 earthquakes with 124 events of magnitude less than 2, 63 events of magnitude 2–3, and 21 events of magnitude 3–4. Recently, on 13 March 2017, an earthquake of *M*<sub>w</sub> 4.1 struck the northern part of the Cambay rift with its epicenter near Tharad ridge (Fig. 1). The earthquake was felt widely in and around Tharad and Sanchor. Moderate seismicity is noticed toward the northeast of the Tharad ridge, where 83 events of magnitude  $< 2$ , 16 events of magnitude 2–3, and 10 events of magnitude 3–4 have occurred since 2007. The Patan block of the Cambay rift is also moderately active; 20 earthquakes (**M** > 2.0) have been recorded there in the recent past with one earthquake of magnitude 4.2 recorded in 2010. Nevertheless, we also investigated the depth distribution of these earthquakes (Fig. 3c). We see that the earthquakes occurred at a depth of 25 km, but most of the events occurred in the range 5–15 km (Fig. 3c). Joshi *et al.* (2017), while doing the joint modeling of the velocity structure and hypocentral locations, reported the focal depths to be around 5–15 km in the Cambay region. It is worth mentioning that Kaila *et al.* (1990) and Dixit *et al.* (2010) reported lower crustal layer at 20–25 and 23–25 km in the northern and southern parts of the Cambay basin, respectively. We also notice that almost all the earthquakes have occurred below 23 km, which is an average depth of the rift pillow in the lower crust (Kaila *et al.*, 1990; Dixit *et al.*, 2010).

We used the broadband records of some seismic stations of GSNet (Chopra *et al.*, 2008) to determine the focal mechanism solutions of few earthquakes with *M*<sub>w</sub> 3.0–4.2 that have occurred in the northern part of the Cambay basin and adjoining region during 2010–2017 (Fig. 4a). To determine the focal mechanism, we conducted moment tensor (MT) inversion using ISOLated Asperities (ISOLA) code (Sokos and Zahradník, 2006). For the inversion, we used broadband data of minimum four nearby stations of the GSNet. The Green's functions are computed at local and regional distances using the discrete wavenumber summation method of Bouchon (1981) and Coutant (1989). The MT solution is obtained using the inverse problem formulation of Kikuchi and Kanamori (1991) by minimizing the difference between the observed and the synthetic displacement in the least-squares sense. The observed and the synthetic waveforms are then matched using the cross-correlation approach with the criterion of obtaining minimum mismatch error. The input of the ISOLA code is the band-passed (minimum 0.04 Hz and maximum 0.18 Hz) velocity records, which are later integrated to obtain displacement traces. Finally, these displacement traces are used as inputs for the MT inversion. The region-specific velocity model of Joshi *et al.* (2017), shown in Table 1, is used in the analysis. The faulting mechanisms

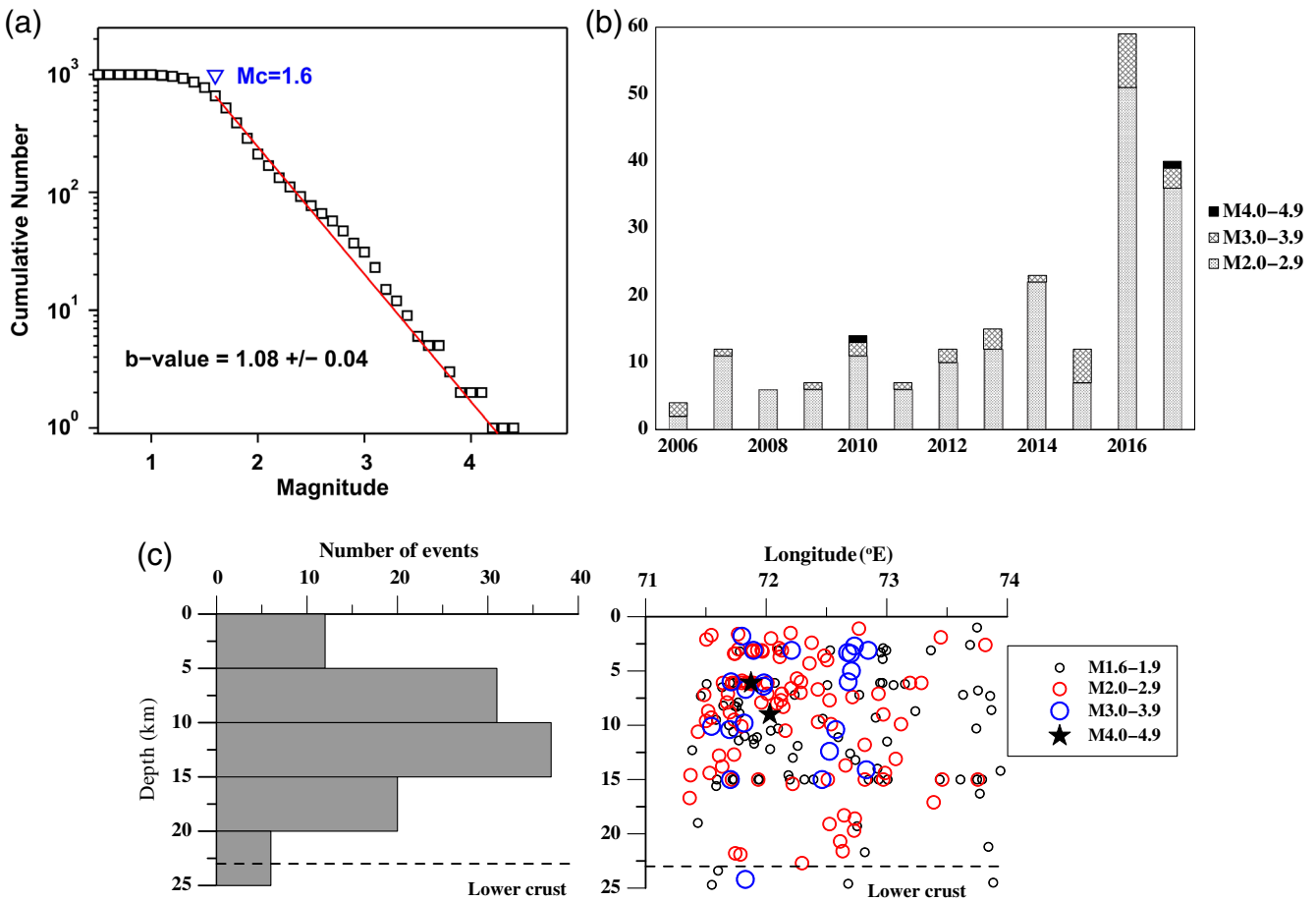


**Figure 3.** (a) Magnitude of completeness of earthquakes in Cambay basin. (b) Histogram of earthquakes of  $M \geq 2.0$  recorded by the ISR network since its inception. The key depicting magnitudes of the earthquakes is shown above. (c) Histogram of the depth distribution of earthquakes (left) and depth distribution of earthquakes ( $M \geq 1.6$ ) along longitude (right). It is observed that the focal depth of most of the earthquakes is  $<20$  km, barring a few. The color version of this figure is available only in the electronic edition.

of eight earthquakes (magnitude range 3.0–4.2 and depth range 3.0–25.0 km) are determined and shown as focal mechanism plots in Figure 4a, and the focal mechanism parameters are presented in Table 2. We chose eight earthquakes based on the signal-to-noise ratio and the waveform match between the observed and the synthetic seismograms. As an example, the waveform comparison of an  $M_w$  4.1 earthquake is shown in Figure 4b. The focal mechanism of this earthquake is estimated using records of four stations in Kachchh, namely, Gadhada (GDD), Suvai (SUV), Badargarh (BDR), and Shivlekha (SIV). For BDR and SIV, which are located in the extreme south of the epicenter, little larger amplitude is noticed in the north-south components, which may be due to the directivity and local site effect. It is observed that most of the earthquakes in the region are predominantly normal with a strike-slip component, barring two events in the eastern part of the basin, which are purely strike slip. The MT solutions provide two nodal planes, trending northeast-southwest and northwest-southeast, with a dip in the range  $50^\circ$ – $60^\circ$  (Fig. 4a). The figure also presents the

$P$  and  $T$  axes of a few earthquakes in the region. The strike direction obtained from focal mechanisms is shown in Figure 4c, revealing major direction toward northeast-southwest. It is evident from Figure 4c that the direction of the strike of the nodal planes of most of the earthquakes is in line with the direction of the Indian plate motion (Fig. 5). We assume the northwest-southeast trend as the strike direction of the auxiliary nodal plane.

#### Horizontal GPS Velocities and Estimation of Strain Rates

A dense network of 22 permanent GPS stations has been established by the ISR in Gujarat. This network is designed for crustal deformation monitoring in Gujarat (Choudhury and Kumar, 2016). Of these 22, four stations are situated near Cambay rift (Fig. 5), namely, Radhanpur (RADP), Dharoi (DHAR), Mount Abu (MABU), and Sipu (SIPU). We have made use of the data of these four stations for estimating deformation in the Cambay region. For the processing of

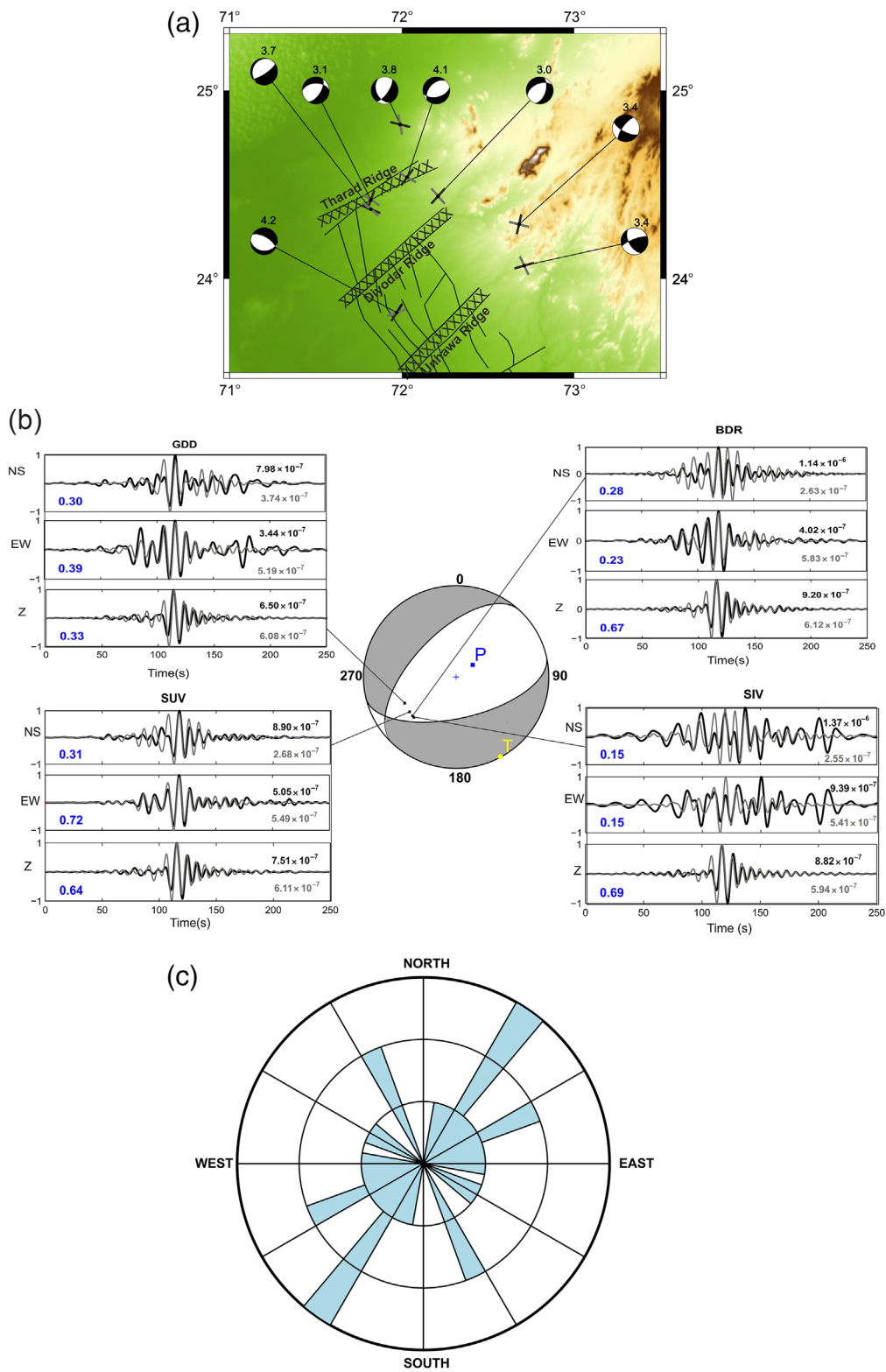


**Figure 4.** (a) Fault plane solutions of eight ( $M \geq 3.0$ ) earthquakes in the Cambay basin with the direction of  $P$  (black) and  $T$  (gray) axes. The numeric value corresponds to the magnitude of the event. The basement ridges are shown after Kaila *et al.* (1990). (b) Centroid moment tensor solution of an  $M_w 4.1$  earthquake that occurred on 13 March 2017 and waveform match between the observed (black) and the synthetic (gray) seismogram at some stations. The normalization factor used for plotting is shown for each component at every station both for the observed and synthetic seismograms. The Yaxis corresponds to displacement (in meters). The variance reduction factor is written. The  $P$  and  $T$  axes correspond to the directions of minimum ( $T$ ) and maximum compressive ( $P$ ) stress. (c) Rose diagram of strike angles of nodal planes of the earthquakes shown in (a). BDR, Badgarh; GDD, Gadhada; SIV, Shivlekhla; SUV, Suvali. The color version of this figure is available only in the electronic edition.

**Table 1**

Velocity Model after Joshi *et al.* (2017) Used in the Present Work

Depth (km)	$V_p \pm \sigma$ (km/s)	$V_s \pm \sigma$ (km/s)
0.0	3.01 ± 0.57	1.74 ± 0.43
4.0	6.21 ± 0.09	3.59 ± 0.01
10.0	6.30 ± 0.04	3.64 ± 0.03
14.0	6.54 ± 0.12	3.78 ± 0.03
18.0	6.70 ± 0.02	3.87 ± 0.01
24.0	7.06 ± 0.10	4.08 ± 0.02
30.0	7.32 ± 0.12	4.23 ± 0.03
34.0	7.88 ± 0.14	4.55 ± 0.13

$V_p$ , P-wave velocity;  $V_s$ , S-wave velocity;  $\sigma$ , standard deviation.

the GPS data, the raw data are converted into the receiver independent exchange format using the program translation, editing, and quality control, which is distributed on the Internet by the University NAVSTAR Consortium (UNAVCO). The GPS data were organized into 24 hr segments covering a UTC day to facilitate the integration of data from 12 surrounding International GNSS Service (IGS) sites, namely, Bangalore (IISC), Bahrain (BAHR), Diego Garcia (DGAR), Kitab (KIT3), Kunming (KUNM), Nanyang (NTUS), Poligan (POL2), Hyderabad (HYDE), Selezaschita (SELE), Bakosurtanal (BAKO), Cocos (COCO), and Wuhan (WUHN). The GPS data collected were processed for the period 2009–2016 using GAMIT/GLOBK 10.6 software to estimate time series of station coordinates and their velocities (King and Bock, 2006; Herring *et al.*, 2010a,b). The coordinates and velocities of all sites were estimated in the International Terrestrial Reference Frame2008 (ITRF2008) by stabilizing IGS reference stations using GAMIT/GLOBK, GLORG. The obvious outliers were removed and down-weighted, and a combined solution to obtain a consistent set of coordinates and their velocities for all the stations was estimated. The horizontal velocities of all the stations were estimated in the ITRF2008 reference frame after combining daily solutions of the sites along with IGS sites. The observed velocities of the four stations in ITRF2008 are in the range of  $49\text{--}50 \pm 0.1$  mm/yr in N47°–49°E (Fig. 5). For the calculation of deformation rates, the motion of the Indian tectonic plate provided by Mahesh *et al.* (2012) was subtracted from

the motion of each site. The residual motion is now considered as the actual rate of deformation at each site. The rates of deformation estimated with respect to Mahesh *et al.* (2012) at the four sites show very small movement of the order of  $1\text{--}1.8 \pm 0.1$  mm/yr in southeast direction (Fig. 5). The site RADP, which is closer to the rift (in the west of WCBM), shows comparatively higher deformation rate  $\sim 1.8$  mm/yr than that of the other sites away from the rift. Although there is a minor difference in the velocities, the directions are similar except at SIPU, which shows dominantly southward motion.

The GPS velocities can also be used to assess other aspects of infinitesimal deformation such as dilatations, rotations, and strains. Cardozo and Allmendinger (2009) developed a Macintosh application SSPX to compute the strain from displacement or velocity data. SSPX uses 2D (or 3D) horizontal velocity components to determine best-fitting strain tensors. The strain depicts the distortion of shape, which can be defined by as few as three points. The triangle as a whole can move as a rigid block. We can measure this deformation, whether it is a strain, translation, rotation, or any combination of them. We used the SSPX software (Cardozo and Allmendinger, 2009) to study characteristics of horizontal crustal strains using the velocities derived from the GPS position time series. In the solution, a uniform grid was constructed for the study area, and the velocity gradients were calculated at each node in the grid. We calculated the strain at the center of each square cell using the distance-weighted method. All four stations are used in the calculation, but the velocities from the GPS stations were weighted with respect to their distance from the grid node with a function  $\alpha$  that specifies how the station effect would decay with distance from the grid node (Shen *et al.*, 1996). In our case,  $\alpha$  and the grid spacing are taken as 40 and 20 km, respectively. These parameters are chosen such that the error in the computed strain value is minimum. The distance-weighted method of SSPX is very effective, particularly for visualizing the regional patterns as indicated by Cardozo and Allmendinger (2009). Cardozo and Allmendinger (2009) computed the strain in Tibet and the Himalayas and the western United States using the distance-weighted routine. It is mentioned that the stations within  $1\alpha$  distance contribute

**Table 2**

Focal Mechanism Parameters of the Eight Earthquakes Estimated in the Present Study

Event Number	Date (yyyy/mm/dd)	Latitude (°N)	Longitude (°E)	Depth (km)	$M_w$	Nodal Plane	Strike (°)	Dip (°)	Rake (°)
1	2010/09/02	23.82	71.97	12.0	4.2	1, 2	300, 94	63, 30	-77, -114
2	2017/03/13	24.54	72.03	9.0	4.1	1, 2	223, 77	46, 50	-115, -66
3	2010/10/24	24.82	71.99	7.0	3.8	1, 2	35, 153	69, 39	-56, -145
4	2015/06/28	24.37	71.82	10.0	3.7	1, 2	203, 56	16, 76	-122, -81
5	2015/03/19	24.05	72.71	4.0	3.4	1, 2	249, 150	77, 56	35, 164
6	2016/05/12	24.29	72.68	6.0	3.4	1, 2	216, 118	71, 68	-157, -20
7	2015/06/28	24.42	71.82	25.0	3.1	1, 2	269, 32	46, 60	-43, -127
8	2014/11/19	24.44	72.21	3.0	3.0	1, 2	18, 247	54, 48	-24, -53

$M_w$ , moment magnitude.

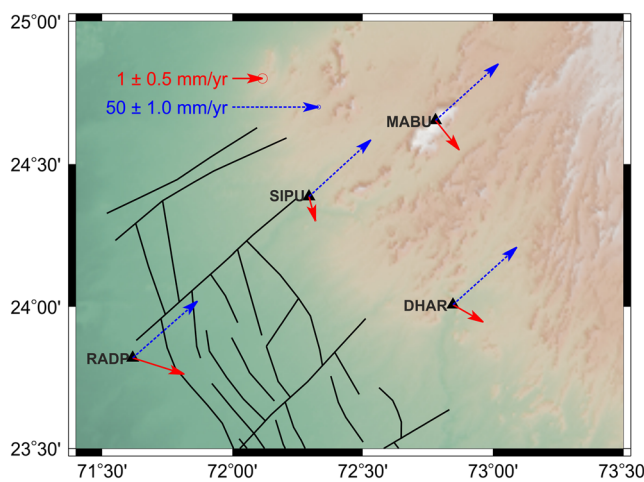


**Figure 5.** Locations of Global Positioning System (GPS) stations (RADP, SIPU, MABU, and DHAR) indicating velocities in International Terrestrial Reference Frame2008 (ITRF2008) (blue dashed arrow) and Indian reference frame (red solid arrow) in northern Cambay rift. The error ellipses are shown at the tip of the vectors. The deformation rates are  $49\text{--}50 \pm 0.1$  and  $1\text{--}1.5 \pm 0.1$  mm/yr in ITRF2008 and Indian reference frame, respectively. The color version of this figure is available only in the electronic edition.

>67% to the solution (Cardozo and Allmendinger, 2009; Shen *et al.*, 1996).

The location and velocity deduced from data of four GPS stations—that is, RADP, SIPU, MABU, and DHAR—are provided as inputs, and the principal axes and principal strains at every grid point are deduced (Fig. 6). The horizontal infinitesimal strain rate is decomposed into two principal horizontal strain axes: shortening and extension axes. The maximum rate of shear strain is a measure of the overall magnitude of the rate of strain in a region and is oriented at  $45^\circ$  to the principal axes. Figure 6 shows the orientation of the shortening and the extension axes and shear-strain rates. The insignificant cells and the strain values outside the network are not shown. We notice that the predominant strain is approximately northwest–southeast extension, accompanied by small northeast–southwest contraction, implying a combination of normal and strike-slip faulting. The maximum shear-strain rates were calculated by dividing the accumulated strains with the time intervals. The maximum shear-strain rate ranges from 0.02 to 0.03 microstrain/yr (Fig. 6). It is found that the highest strain rate prevailing around the Diyodar ridge, and the spatial pattern probably indicate an increasing trend toward the Tharad ridge, which is also seismically the most active part of the studied region (Fig. 6). Unfortunately, it is not possible to constrain the strain values around Tharad ridge because there is no GPS station nearby.

## Discussion

The entire CRB is not seismically active. The northern part of the rift, where it merges with Kachchh rift, is seismically the most active region and has produced moderate

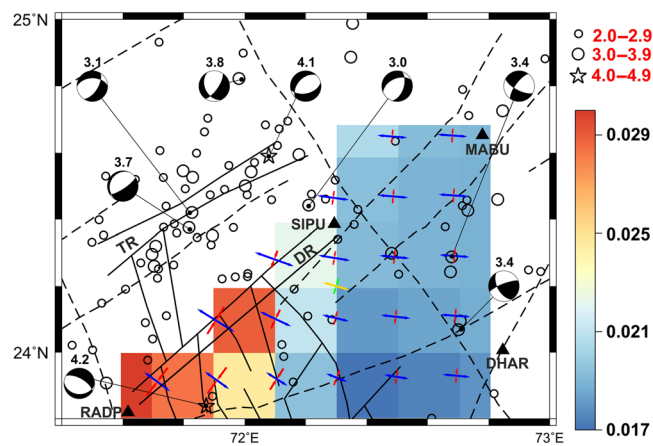


**Figure 6.** GPS-derived strain rates and shear-strain rates in microstrain per year. The locations of the GPS stations are shown by triangles. Crosses indicate orientation and magnitude of maximum (blue) and minimum (red) horizontal strain rates deduced by distance-weighted method. The best fit is shown as yellow (extension) and green (shortening) axes. The area shows dominantly extensional strain. The earthquake mechanisms are shown by focal mechanism plots. The numerical value on each focal mechanism plot indicates the magnitude of the earthquake. Locations of earthquakes of  $M$  3–3.9 and 2–2.9 are shown by bigger and smaller open circles, respectively. Black stars show locations of the earthquake of  $M$  4.0–4.9 as shown in the legend. The lineaments are marked by dashed lines. DR, Diyodar ridge; TR, Tharad ridge. The color version of this figure is available only in the electronic edition.

earthquakes in the historical past. In recent times, too, most of the earthquakes occurring in the rift are clustered in this region (Fig. 1). Kaila *et al.* (1990) mapped three basement ridges within the Cambay basin: Tharad, Diyodar, and Unhawa (Fig. 1). The spatial distribution of the seismicity of the Cambay basin depicts that most of the earthquakes in the region are clustered along the transverse ridges oriented in the northeast–southwest direction and sympathetic to the Delhi–Aravalli trend, called the Sanchor–Patan block (Fig. 2). We also note that the western shoulder of the Cambay rift comprising the RAD arch and the extension of west coast lineament has considerable seismicity. The 600 km long west coast lineament trending toward northwest–southeast is the continuation of the east Cambay fault after dextral offset by the Narmada faults (Biswas, 1982, 1987). Moreover, the eastern shoulder of the rift comprising Jaisalmer–Barwani lineament has recorded many micro-earthquakes (Fig. 1). It is around 1000 km long lineament and extends from Barwani in the southeast to Jaisalmer in the northwest. In addition, a number of lineaments (e.g., Chambal–Jamnagar and Pisanganga–Vadnagar) crisscrossing the entire region to the east of Cambay rift are active. Mostly, the seismicity is concentrated where these lineaments crisscross with each other (Fig. 1). These lineaments can be traced for hundreds of kilometers in the area and have controlled the neotectonic activities in this region (Roy and Jakhar, 2002).

We observe from the estimated fault plane solutions that the earthquakes in the Cambay rift and its nearby region predominantly show normal mechanism with secondary strike-slip component (Fig. 4a). The earthquakes away from the rift show strike-slip mechanism (Fig. 4a). The strike is predominantly northeast–southwest and dips 50°–60°. The focal mechanism analysis shows that extensional tectonics dominate in the region. The GPS-derived strain tensors also show the dominance of extensional tectonics (Fig. 6). It is noteworthy that eight years (2009–2016) of continuous data of four GPS observations have provided information about the amount of strain accumulating in the region. The spatial distribution of the shear-strain rate shows the maximum strain of ~0.03 microstrain/yr in the area around the Diyodar ridge and north of the Unhawa ridge, where considerable seismicity is also noticed (Fig. 6). In addition, we see relatively high strain rates around Radhanpur arch (~0.03 microstrain/yr) and the eastern part of the rift (0.02 microstrain/yr) (Fig. 6). In this context, we mention that [Talwani \(1999\)](#), while studying fault geometry and earthquakes in the interiors of the tectonic plate, found that the interiors or rigid plate deform generally at a rate of  $10^{-10}$ – $10^{-9}$  strain/yr. However, at intersecting fault zones or stress concentrators, strain accumulates at a rate of  $10^{-8}$ – $10^{-7}$  strain/yr. Therefore, we infer that the high rates of strain in this part may have a linkage with the intersecting lineaments or stress concentrators. The northwest–southeast extensional motion along with shortening in a northeast–southwest direction is revealed by the GPS-derived strain tensor (Fig. 6). The direction of  $P$  and  $T$  axes of the earthquakes also shows nearly northwest–southeast extension along with northeast–southwest compression (Fig. 4a). Both the fault plane solutions and the GPS-derived strain tensors suggest a prominent extension (Fig. 6), surprisingly, in a compressional regime. The focal mechanisms of historical earthquakes in this region indicate dominant horizontal contraction ([Chandra, 1978, 1977](#)). Moreover, [Gangopadhyay and Talwani \(2003\)](#) reported the type of faulting observed for the rift-associated intraplate regions, including Gujarat. They found that the main style of faulting is strike slip, reverse, or a combination of both.

We notice that the region in and around the Tharad ridge comprising north and south Sanchor basins, which is interpreted as basement high by [Kaila et al. \(1990\)](#), is seismically most active at present (Figs. 1 and 6). Although GPS measurements cannot quantify the strain rates because of the lack of data, the present trend indicates a high strain rate in this part of the basin. The Kachchh and Cambay rifts intersect at the northern part of the Cambay basin, which is a part of a failed rift, consisting of Precambrian ridges ([Kaila et al., 1990](#)). A recent study by A. K. Chouhan *et al.* (unpublished manuscript, 2019, see [Data and Resources](#)) through modeling of European Improved Gravity model of the Earth (EIGEN-6C4) gravity data reported signatures of thin crust and high-density underplating layer beneath the CRB. [Sharma et al. \(2018\)](#) also presented seismic evidence of the magmatic underplating through surface-wave tomography

in the Saurashtra, Kachchh, Cambay, and Narmada rift regions. [Kaila et al. \(1990\)](#) and [Dixit et al. \(2010\)](#), on the basis of seismic refraction and reflection data, reported a high-velocity (7.2–7.5 km/s) crustal layer at 23–25 km depth that extends up to the Moho (31–37 km). They interpreted the formation of this high-velocity layer as a result of magmatic underplating during mantle upwelling, rifting, and large-scale Deccan extrusions. [Dixit et al. \(2010\)](#) modeled this high-velocity, 10- to 12-km-thick layer as a rift pillow-shaped body. This rift pillow may be formed as a result of magmatic intrusion. The same was found beneath most of the continental rifts such as the East-African rift, Rio Grande rift, Rhine graben, and Salton trough, to name a few ([Dixit et al., 2010](#)). The range of size and the velocity may differ beneath these rifts, but the presence of rift pillows in the continental rifts is common ([Gangopadhyay and Talwani, 2003](#)). [Gupta \(1981\)](#) also found that the high-heat flow and high-Bouguer anomaly in the Cambay support the presence of an intrusive body. He modeled the shape and size of this intrusive igneous body and found that it may be in the shape of a rectangular mass of about 40–50 km wide and at a depth of 10 km beneath Mehsana area, narrowing down toward the northern part of the Cambay basin. The adjacent Kachchh rift also has an ultramafic plutonic rift pillow resting at the base of the lower crust ([Biswas, 2005](#)). It was observed that all major rifts in the world pass through three stages: crustal thinning and consequent uparching of the mantle during the prebreakup crustal distension, fracturing of mantle lithosphere boundary and melting to form a mafic igneous body (rift pillow) in the lower lithosphere, and rupturing of the upper crust forming the rifted basin ([Zeigler, 1992](#)). There is evidence of deep-seated mafic plutons along the rift axis of the Cambay basin, which is believed to be the Reunion hot spot trail ([Raval, 1989](#)); this is confirmed by high heat flow and high Bouguer anomaly (B. S. Negi, unpublished manuscript, 1952, see [Data and Resources](#); [Sengupta, 1967](#)).

The presence of basement ridges and magmatic material in the form of a rift pillow in the lower crust is combinedly responsible for the continuous accumulation of the strain energy. The focal depths of the earthquakes apparently indicate the occurrence of an earthquake in the upper and the lower crusts and above the rift pillow in this region (Fig. 3c). [Gangopadhyay and Talwani \(2003\)](#), after studying symptomatic features of 39 intraplate earthquakes worldwide, found that in stable continental regions (SCRs), tectonic stresses caused by plate movement buildup localized stresses at pre-existing zones, where stresses build up such as failed rifts, fault intersections, buried plutons, rift pillows, and ridges. The plate motion causes stresses to build up near these stressed regions, which ultimately releases in the form of earthquakes. It has also been observed that 64% of all the earthquakes in SCR are in extensional basins or grabens. However, plate boundary interactions are not the primary sources of the stress here. We anticipate a little different mechanism in the Cambay graben.

Recently, Danda and Rao (2019) conducted magnetotelluric measurements along the four profiles (total of 68 stations) across the CRB and confirmed the presence of a thick conductive layer (~2000–7500 S). In addition, Danda *et al.* (2017), through broadband and long-period magnetotelluric study, have identified a highly conductive (~1000 S) layer within the Cambay rift zone. They argued that the delineated crustal conductors may be related to the presence of fluids associated with fault and shear zones. Their resistivity model shows substantial contrasts in the resistivity values (1–10,000  $\Omega$ m) from west to the east, indicating a heterogeneous subsurface structure. We assume that a differential vertical stress can be induced because of the heterogeneity. Furthermore, we believe that the flow of fluid under the compression results in stretching, causing an extensional regime, although it cannot be mathematically demonstrated. In other words, the ambient stress field is altered substantially by lateral heterogeneity caused by fluids and flow of magmatic materials in the lower crust. This could be a reason for the occurrence of normal earthquakes as revealed by the focal mechanisms and supported by geodetic strain tensors (Fig. 6).

The average strain rate in and around Cambay rift is of the order of  $2 \times 10^{-8}$  strain/yr. This rate is comparable to the average strain in the nearby seismically very active Kachchh rift, where the value is  $5 \times 10^{-8}$  strain/yr (Reddy and Sunil, 2008; Kothiyari *et al.*, 2016). The geodetic moment rate can be obtained using the strain rate (Kostrov, 1974), and the maximum magnitude can be inferred using the geodetic moment rate. Based on the seismotectonic setup and past seismicity, the area falls under zones III and IV on the seismic zoning map of India (BIS, 2002), where magnitudes of the MCEs are 6 and 7, respectively. This is a general understanding. Therefore, we thought it was necessary to evaluate the maximum magnitude using the strain rates estimated in this study. Ramalingeswara Rao (2002) established a relationship between maximum magnitude ( $M_{\max}$ ) and the strain rate ( $\dot{\epsilon}$ ) for the Indian shield as follows:

$$M_{\max} = (7.52 \pm 0.12) + (0.18 \pm 0.014) \log \dot{\epsilon}. \quad (2)$$

Using equation (2) and considering an average strain rate of  $2 \times 10^{-8}$  strain/yr, the calculated  $M_{\max}$  is found to range between 6.1 and 6.4. This estimation appears to be reasonable because it is deduced using the observed GPS information.

Failed rifts, presence of basement ridges, and intrusive bodies are the localized zones, where stresses are built up because of tectonic forces in an intraplate environment. In the CRB, an additional force is combined with the ambient stress field because of the Indian plate motion. However, the seismic potential of this region may not appear to be alarming. Similar to high strain rate areas, low-magnitude earthquakes are expected, but the higher magnitude is unlikely (Riguzzi *et al.*, 2012). The northern part of the CRB shows high strain values, as we see from the strain distribution map (Fig. 6). Therefore, we can expect a large number of small earthquakes in this part of the CRB, but the likelihood of a

strong or major event is dubious. However, the chance of strong earthquakes in the low-strain regions, such as southeast of the CRB, cannot be ruled out. This was indicated by Riguzzi *et al.* (2012), who studied the linkage between the geodetic strain rates with earthquake size in Italy. Our estimation implies that an earthquake of magnitude 6.4 can occur in this area. The high strain rate prevailing in the region calls for the need to closely monitor the deformation field through a dense network of GPS measurements over a long period.

## Conclusions

In recent years, the northern part of the Cambay rift has been experiencing occurrences of many small earthquakes, mostly in the magnitude ranging from 1 to 3 with a maximum of 4.2. In this study, we attempted to investigate the cause of seismicity in the northern part of the Cambay rift. Because the region is a potential zone for hydrocarbon deposits because of the large thickness of tertiary sediments, it has been thoroughly investigated through various geophysical methods, including seismics, gravity, magnetics, and so on. All these measurements found that the region has high heat flow with the possibility of the presence of magmatic material in the form of rift pillow in the lower crust. We observed that most of the seismicity in the northern part of the rift is clustered along the basement high and ridges striking along the Delhi–Aravalli trend, which crisscrosses the Cambay rift. This is also the region where east–west-trending Kachchh rift ends against the hinterland of north–northwest–south–southeast-trending Radhanpur–Barmer ridge, which is the western rift shoulder of Cambay rift. The strain measurements in the area using continuous GPS observations have shown that the northern part of the Cambay rift is comparatively highly strained with a maximum strain of around 0.03 microstrain/yr, comparable to the strain rates of seismically most active Kachchh basin. Surprisingly, the fault mechanisms and GPS-derived strain tensors reveal that the area, where compression is more likely, is undergoing extension. We notice an increasing trend of the strain rates in the northern part of the basin, where the highest seismicity is also observed. However, the quantification of the strain is not possible due to the lack of GPS observations.

Failed rifts, the presence of basement ridges, and intrusive bodies in a region are the zones where stresses are built up because of tectonic forces in an intraplate environment. We conclude that in the CRB, an additional component of stress distinct from the plate boundary stress is overlaid on the regional stress field. These highly stressed zones are very localized. This stress is occasionally released in the form of earthquakes. Using the estimated strain rate prevailing in the region, we may expect an earthquake of magnitude up to 6.4. We emphasize the need to monitor the strain rates in such regions closely through a dense network of permanent GPS and seismograph stations. Long-period and systematic GPS observations may provide more useful information on the enigmatic behavior of earthquakes in this region.

## Data and Resources

The earthquake data used in this study have been obtained from the Gujarat seismological network (GSNet) operated by the Institute of Seismological Research (ISR), Gandhinagar, India. The Global Positioning System (GPS) data are obtained from permanent GPS stations operated by the ISR, Gandhinagar, India. The data are available to researchers in collaborative mode and may be obtained by contacting the authors. The unpublished manuscripts by A. K. Chouhan, P. Choudhury, and S. K. Pal (2019), "New evidence for a thin crust and magmatic underplating beneath the Cambay rift basin, western India through modelling of EIGEN-6C4 gravity data," submitted to *J. Earth. Syst. Sci.* and B. S. Negi (1952), "Gravity and magnetic survey in subsurface structures in the Borsad area, Khera district," submitted to *Geol. Surv. India Rep.*

## Acknowledgments

The authors wish to thank the Director General, Institute of Seismological Research (ISR) for the helpful discussions and his permission to publish this work. The authors also thank Santosh Kumar and Rakesh Dumka for running and maintaining the broadband seismic (BBS) and Global Positioning System (GPS) network. The funding agencies, Department of Science and Technology, Government of Gujarat and Ministry of Earth Sciences, Government of India are gratefully acknowledged. The authors acknowledge Vishwa Joshi for providing the catalog of Cambay region. The authors sincerely acknowledge the thoughtful comments of Will Levandowski, which greatly enhanced the quality of the article. The article was improved by constructive reviews by Editor-in-Chief Thomas Pratt and Associate Editor YoungHee Kim and two anonymous reviewers.

## References

- Bureau of Indian Standards (BIS) (2002). *IS 1893 (Part 1)-2002: Indian Standard Criteria for Earthquake Resistant Design of Structures: Part 1 - General Provisions and Buildings*, Bureau of Indian Standards, New Delhi, India.
- Biswas, S. K. (1982). Rift basins in western margin of India with special reference to hydrocarbon prospects, *Bull. Am. Assoc. Petrol. Geol.* **66**, 1497–1513.
- Biswas, S. K. (1987). Regional tectonic framework, structure and evolution of the western margin basins of India, *Tectonophysics* **135**, 307–327.
- Biswas, S. K. (2005). A review of structure and tectonics of Kutch basin, western India with special reference to earthquakes, *Curr. Sci.* **88**, 1592–1600.
- Biswas, S. K. (2012). Status of petroleum exploration in India, *Proc. Ind. Natl. Sci. Acad.* **78**, 475–494.
- Biswas, S. K. (2014). Active tectonics of western continental margin of Indo-Pak craton—stress source for SCR earthquakes, *J. Earthq. Sci. Eng.* **1**, 46–58.
- Bouchon, M. (1981). A simple method to calculate Green's functions for elastic layered media, *Bull. Seismol. Soc. Am.* **71**, 959–971.
- Cardozo, N., and R. W. Allmendinger (2009). SSPX: A program to compute strain from displacement/velocity data, *Comput. Geosci.* **35**, 1343–1357.
- Chandra, U. (1977). Earthquakes of Peninsular India—A seismotectonic study, *Bull. Seismol. Soc. Am.* **67**, no. 5, 1387–1413.
- Chandra, U. (1978). Seismicity, earthquake mechanics and tectonics along the Himalayan mountain range and vicinity, *Phys. Earth Planet. In.* **16**, 109–131.
- Chopra, S., R. B. S. Yadav, H. Patel, S. Kumar, K. M. Rao, B. K. Rastogi, A. Hameed, and S. Srivastava (2008). The Gujarat (India) seismic network, *Seismol. Res. Lett.* **79**, 799–808.
- Choudhury, P., and M. R. Kumar (2016). The Institute of Seismological Research—A premier research center for seismology in India, *Proc. Ind. Natl. Sci. Acad.* **82**, no. 3, 1049–1060.
- Coutant, O. (1989). Program of numerical simulation AXITRA, *Res. Rept.*, Laboratoire de Géophysique Interne et Tectonophysique, Grenoble, France.
- Danda, N., and C. K. Rao (2019). Magnetotelluric study to characterize sediment thickness across Kachchh and Cambay rift basins, western India, *Curr. Sci.* **16**, no. 2, 299–304.
- Danda, N., C. K. Rao, and A. Kumar (2017). Geoelectric structure of northern Cambay rift basin from magnetotelluric data, *Earth Planets Space* **69**, 140.
- Dixit, M. M., H. C. Tewari, and C. V. Rao (2010). Two-dimensional velocity model of the crust beneath the South Cambay Basin, India from refraction and wide-angle reflection data, *Geophys. J. Int.* **181**, 635–652.
- Gangopadhyay, A., and P. Talwani (2003). Symptomatic features of intraplate earthquakes, *Seismol. Res. Lett.* **74**, 863–883.
- Gupta, M. L. (1981). Surface heat flow and igneous intrusion in the Cambay basin India, *J. Volcanol. Geoth. Res.* **10**, 279–292.
- Gutenberg, B., and C. F. Richter (1944). Frequency of earthquakes in California, *Bull. Seismol. Soc. Am.* **34**, 185–188.
- Havskov, J., and L. Ottemöller (1999). SEISAN earthquake analysis software, *Seismol. Res. Lett.* **70**, no. 5, 532–534.
- Herring, T. A., R. W. King, and S. C. McClusky (2010a). *Documentation of the GAMIT GPS Analysis Software Release 10.4*, Department of Earth and Planetary Sciences, Massachusetts Institute of Technology, Cambridge, Massachusetts.
- Herring, T. A., R. W. King, and S. C. McClusky (2010b). *GLOBK, Global Kalman Filter VLBI and GPS Analysis Program, Version 10.4*, Department of Earth and Planetary Sciences, Massachusetts Institute of Technology, Cambridge, Massachusetts.
- Joshi, V., S. Chopra, P. Mahesh, and S. Kumar (2017). Joint modeling of velocity structure and hypocentral locations in the seismically active Kachchh, Saurashtra, and Narmada regions of Western India: An active intraplate region, *Seismol. Res. Lett.* **88**, no. 5, 1390–1402.
- Kaila, K. L., H. C. Tewari, V. G. Krishna, M. M. Dixit, D. Sarkar, and M. S. Reddy (1990). Deep seismic sounding studies in the north Cambay and Sanchor basins, India, *Geophys. J. Int.* **103**, 621–637.
- Kikuchi, M., and H. Kanamori (1991). Inversion of complex body waves-III, *Bull. Seismol. Soc. Am.* **81**, 2335–2350.
- King, R. W., and Y. Bock (2006). *Documentation of the GAMIT GPS Analysis Software*, Massachusetts Institute of Technology, Cambridge, Massachusetts.
- Kostrov, V. V. (1974). Seismic moment and energy of earthquakes, and seismic flow of rock, *Izv. Acad. Sci. USSR Phys. Solid Earth* **1**, 23–44.
- Kothiyari, G. C., R. K. Dumka, A. P. Singh, G. Chauhan, M. G. Thakkar, and S. K. Biswas (2016). Tectonic evolution and stress pattern of south Wagad fault at the Kachchh Rift basin in western India, *Geol. Mag.* **154**, 875–887, doi: [10.1017/S0016756816000509](https://doi.org/10.1017/S0016756816000509).
- Kundu, J., and M. R. Wani (1992). Structural style and tectono-stratigraphic framework of Cambay rift basin, Western India, *Int. J. Petrol. Geol.* **1**, no. 2, 181–202.
- Mahesh, P., J. K. Catherine, V. K. Gahalaut, B. Kundu, A. Ambikapathy, A. Bansal, L. Premkishore, M. Narsaiah, S. Ghavri, R. K. Chadha, et al. (2012). Rigid Indian plate: Constraints from GPS measurements, *Gondwana Res.* **22**, 1068–1072.
- Mathur, L. P., K. L. N. Rao, and A. N. Chaubey (1968). Tectonic framework of Cambay basin, India, *Bull. Oil Nat. Gas Comm.* **5**, 7–28.
- Rajendran, C. P., and K. Rajendran (2001). Characteristics of deformation and past seismicity associated with the 1819 Kutch earthquake, northwestern India, *Bull. Seismol. Soc. Am.* **91**, 407–426.
- Ramalingeswara Rao, B. (2002). Historical seismicity and deformation rates in the Indian Peninsular Shield, *J. Seismol.* **4**, 247–258.

- Rastogi, B. K., S. Kumar, and S. K. Aggrawal (2013). Seismicity of Gujarat, *Nat. Hazards* **65**, 1027–1044.
- Raval, U. (1989). On hotspots, Meso-Cenozoic tectonics and possible thermal networking beneath the Indian subcontinent, *Proc. Sem. on Geophys. Res. in India. Indian Geophys. Union*, 314–330.
- Reddy, C. D., and P. S. Sunil (2008). Post-seismic crustal deformation and strain rate in Bhuj region, western India, after the 2001 January 26 earthquake, *Geophys. J. Int.* **172**, 593–606.
- Riguzzi, F., M. Crespi, R. Devoti, C. Doglioni, G. Pietrantonio, and A. R. Pisani (2012). Geodetic strain rate and earthquake size: New clues for seismic hazard studies, *Phys. Earth Planet. In.* **206/207**, 67–75.
- Roy, A. B., and S. R. Jakhar (2002). *Geology of Rajasthan (Northwest India Precambrian to Recent)*, Scientific Publishers, Jodhpur, India, 421 pp.
- Sengupta, S. N. (1967). Structure of the Gulf of Cambay, *Proc. Symp. Upper Mantle Project*, Hyderabad, India, 334–341.
- Sharma, J., M. R. Kumar, K. S. Roy, and P. N. S. Roy (2018). Seismic imprints of plume-lithosphere interaction beneath the northwestern Deccan Volcanic Province, *J. Geophys. Res.* **123**, 10,831–10,853.
- Shen, Z.-K., D. D. Jackson, and B. X. Ge (1996). Crustal deformation across and beyond the Los Angeles basin from geodetic measurement, *J. Geophys. Res.* **101**, 27,957–27,980.
- Sokos, E. N., and J. Zahradník (2006). ISOLA: A Matlab GUI for use with ISOLA Fortran codes, *USER's Guide, Version 2.5*, 34 pp.
- Talwani, P. (1999). Fault geometry and earthquakes in continental interiors, *Tectonophysics* **305**, 371–379.
- Wani, M. R., and J. Kundu (1995). Tectonostratigraphic analysis in Cambay rift basin: Leads for future exploration, *Proc. First International Petro Conference*, B. R. Publishing Corporation, Delhi, India, 147–174.
- Weimer, S., and M. Wyss (2000). Minimum magnitude of complete reporting in earthquake catalogs: Examples from Alaska, the western United States, and Japan, *Bull. Seismol. Soc. Am.* **90**, 859–869.
- Zeigler, P. A. (1992). Geodynamics of rifting and implications in hydrocarbon habitat, *Tectonophysics* **215**, 221–253.

Institute of Seismological Research  
Knowledge Corridor, Raisan  
Gandhinagar 382009  
Gujarat, India  
pallabee.ch@gmail.com  
sumerchopra@isr.res.in  
charukamra007@gmail.com  
rchndas7@gmail.com

Manuscript received 21 May 2019;  
Published Online 15 October 2019